Surface & Coatings Technology 402 (2020) 126347

Contents lists available at ScienceDirect

Surface & Coatings Technology

journal homepage: www.elsevier.com/locate/surfcoat

Understanding the effect of Al/Ti ratio on the tribocorrosion performance of Al/Ti co-doped diamond-like carbon films for marine applications

Xiaowei Xu[a,b], Peng Guo[a], Xiao Zuo[a], Lili Sun[a], Xiaowei Li[a,c,d,*], Kwang-Ryeol Lee[d], Aiying Wang[a,e,f,**]

[a] Key Laboratory of Marine Materials and Related Technologies, Zhejiang Key Laboratory of Marine Materials and Protective Technologies, Ningbo Institute of Materials Technology and Engineering, Chinese Academy of Sciences, Ningbo 315201, PR China
[b] School of Physical Science and Technology, ShanghaiTech University, Shanghai 201210, PR China
[c] School of Materials and Physics, China University of Mining and Technology, Xuzhou 221116, PR China
[d] Computational Science Center, Korea Institute of Science and Technology, Seoul 136-791, Republic of Korea
[e] Center of Materials Science and Optoelectronics Engineering, University of Chinese Academy of Sciences, Beijing 100049, PR China
[f] Ningbo Institute of Industrial Technology, Chinese Academy of Sciences, Ningbo 315201, PR China

ARTICLE INFO

Keywords:
Tribocorrosion
NaCl solution
Synergistic effect
Al/Ti ratio
Diamond-like carbon

ABSTRACT

Al and Ti co-doped diamond-like carbon (DLC) films (Al/Ti-DLC) were prepared through hybrid ion beam deposition technique, in which the Al/Ti ratio was tailored from 6.6 to 2.0. The dependence of tribocorrosion performance of Al/Ti-DLC film on the Al/Ti ratio in 3.5 wt% NaCl solution was systematically explored. Results indicated that the existing states of Al and Ti dopants in the film were independent on the Al/Ti ratio, where Al existed in the form of oxidized state, while Ti mainly bonded with C and thus formed the titanium carbide following the presence of titanium oxide, leading to the increase of hardness and elastic modulus with the decrease of Al/Ti ratio. In particular, with reducing the Al/Ti ratio from 6.6 to 2.0, the tribocorrosion resistance was improved, mainly originating from the reduction of pure mechanical wear. However, EIS analysis further revealed that although the mechanical wear accelerated the electrochemical corrosion of Al/Ti-DLC films, the contribution of the synergistic effect between mechanical wear and corrosion attack to materials loss increased following the drop of Al/Ti ratio, due to the corrosion-induced wear rather than wear-induced corrosion. These outcomes not only shed light on the effect of Al/Ti ratio in the film on the tribocorrosion property but also guide the design of DLC films for marine applications.

1. Introduction

Marine frictional components, such as cylinder, piston rods, bearings, hinges, and other engineering materials [1–3], normally suffer from the combined effect of mechanical wear and chemical corrosion in the harsh marine environment, which is named as tribocorrosion [4–7]. In particular, the total loss of material, which is generated during the tribocorrosion process, is much higher than that caused by the pure mechanical wear or corrosion, respectively, aggravating the failure of marine metal components. So it is of great importance to develop the high-efficient surface protective coating with both the self-lubricating and anti-corrosion capacities, which can exert on the surface of marine key moving components against tribocorrosion failure and thus extend its lifetime and reliable operation. This has already attracted widespread concerns in the past several years.

Due to the superior comprehensive properties (high hardness, good chemical inertness, and excellent tribological property), diamond-like carbon (DLC) film serving as the inorganic protective film has aroused worldwide interest from the scientific and engineering communities in the past few decades [8,9]. For example, Pougoum et al. [10] proved that the tribocorrosion resistance of Fe_3Al coating sprayed using high-velocity oxyfuel could be increased with the addition of DLC top layers during cathodic polarization. Cui et al. [11,12] reported that the existence of multilayered structure with a well-bonded interface endowed the DLC film with a high Warburg impedance value (10^7 Ω·cm^2). While Pu et al. [13] suggested that the appropriate modulation period of multilayer DLC film could significantly raise its tribocorrosion resistance by suppressing the crack propagation. Liu et al. [14] deposited

* Correspondence to: X. Li, Computational Science Center, Korea Institute of Science and Technology, Seoul 136-791, Republic of Korea.
** Correspondence to: A. Wang, Center of Materials Science and Optoelectronics Engineering, University of Chinese Academy of Sciences, Beijing 100049, PR China.
E-mail addresses: lixw0826@gmail.com (X. Li), aywang@nimte.ac.cn (A. Wang).

https://doi.org/10.1016/j.surfcoat.2020.126347
Received 29 May 2020; Received in revised form 17 August 2020; Accepted 22 August 2020
Available online 25 August 2020

DLC film on CoCrMo alloys, which exhibited excellent corrosion resistance as well as tribological performance under simulated biological environment.

In our previous works [15–17], we have synthesized the DLC films with Ti and Al as co-dopants (Al/Ti-DLC) successfully and evaluated the dependence of tribological and electrochemical behaviors on Al/Ti ratio, respectively. However, it still lacks systematic researches on the tribocorrosion performance of Al/Ti-DLC film in the marine environment, in which mechanical wear and corrosion occur in synergism. This limits its application as a protective film on the surface of marine moving components. Consequently, in this study, we tailored the Al/Ti-DLC films with the Al/Ti ratio from 6.6 to 2.0 through the one-step hybrid ion beam (HIB) deposition process. The tribocorrosion behavior of Al/Ti-DLC films with various Al/Ti ratios in 3.5 wt% NaCl solution, especially the synergistic effect between mechanical wear and corrosion attack, was systematically investigated. The underlying mechanism was discussed according to the tribological and electrochemical analysis.

2. Experimental method

2.1. Film preparation

The HIB system was applied to prepare the Al/Ti-DLC films on 316L stainless steel (316L SS) and silicon P (100) wafers substrates, respectively. It contained a linear anode-layer ion source (ALIS) with hydrocarbon gas for carbon deposition and a direct current magnetron sputtering source with Al/Ti composited target for simultaneous co-doping of Al and Ti elements. Especially, the sputtering target consisting of two triangular Ti (99.99%) and Al (99.99%) spliced targets was used in order to tailor the Al/Ti ratio in the film at one-step deposition process [17,18]. All substrates were ultrasonically cleaned 20 min in acetone and then dried with nitrogen. After that, they were placed in the deposition chamber and the distances of substrates from ALIS and sputtering source were kept at around 17.5 cm separately. The schematic diagrams of HIB system, sputtering target, and the placement of substrates in the chamber could be found in previous studies [17,18]. Prior to the deposition process, Ar plasma was applied to etch each sample for 20 min at the bias voltage of −100 V, which could not only raise the bonding strength between DLC film and substrate but also remove the inevitable surface contaminations. Then, hydrocarbon gas, C_2H_2, and Ar were introduced into the ALIS and magnetic sputter separately to deposit the Al/Ti-DLC film; the substrate holder was rotated and its direction was changed every 20 min; the deposition time was 120 min. Table 1 listed the detailed parameters for film deposition.

2.2. Microstructure characterization

The surface profilometer (Alpha-Step IQ) recorded the film thickness and also tested the profile of wear track after tribocorrosion test. Field emission scanning electron microscopy (SEM, FEI Quanta FEG 250) was applied to obtain the morphology of wear track in Al/Ti-DLC film. X-ray photoelectron spectroscopy (XPS, Thermo Scientific ESCALAB 250) was employed to acquire the information about the composition and chemical bond structure of each film after etching its surface for 5 min using Ar ion beam. High-resolution transmission electron microscopy (HR-TEM, FEI Tecnai F20) was used to characterize the microstructure of the film.

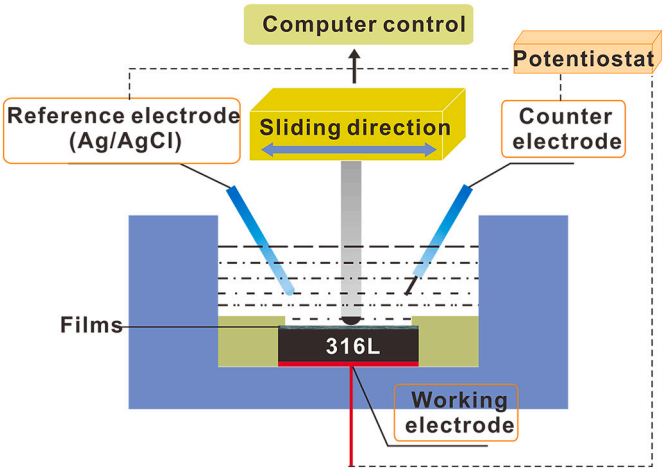

Fig. 1. Schematic diagram of the tribocorrosion apparatus.

2.3. Mechanical, tribocorrosion, and electrochemical investigations

The hardness (H) and elastic modulus (E) of the film were evaluated by Nanoindenter (MTS-G200); the indentation depth was the value equal to the 1/10 thickness of the as-deposited film for the sake of weakening the substrate influence on the tested results, and all of the indentations were conducted six times for each sample. Tribocorrosion property of the Al/Ti-DLC film was evaluated in 3.5 wt% NaCl solution through an integrated apparatus including a reciprocating tribometer (RTEC MFT5000) and an electrochemical workstation, as illustrated in Fig. 1.

Electrochemical test was undertaken in 3.5 wt% NaCl solution by the ModuLab (Solatron Analytical) with a three-electrode electrochemical system at room temperature (25 ± 1 °C). The counter and reference electrodes were platinum sheet and saturated Ag/(AgCl)/KCl, respectively, while the working electrode was Al/Ti-DLC sample which had an exposed area of 2.5 cm^2. Before the test, open circuit potential (OCP) was first evaluated by immersing the film sample into the 3.5 wt % NaCl solution for about 2 h. After that, the potentiodynamic polarization curve was recorded; the sweep rate was 2 mV/s and the scanning potential was from −0.3 V vs SCE to 1.5 V vs. SCE. The electrochemical impedance spectroscopy (EIS) was measured with the range of frequency from 10 kHz to 10 mHz, which was followed by the fitting and quantitative analysis of equivalent circuit (EC) using ZSimpWin software. In order to ensure the repeatability, the electrochemical test of each sample was replicated three times.

For the tribological test of Al/Ti-DLC film, the reciprocating frequency, applied normal load, and wear track length were 2 Hz, 5 N, and 5 mm, respectively. The Si_3N_4 ball (HRC75) as the sliding counter body was used and its diameter was 6 mm; the test time was 3600 s. After tribocorrosion tests, the wear rate was calculated using the Archard equation as follows:

$$K = \frac{V}{L \times N} \quad (1)$$

where K, L, N, and V corresponded to the wear rate (unit: mm^3/Nm), total sliding distance (unit: m), normal load (unit: N), and wear volume loss (unit: mm^3), respectively [19,20]. For each sample, the sliding test was also reproduced at least 3 times to calculate the average wear rate and coefficient of friction (COF) values. In addition, the tribological test

Table 1
Detailed experimental parameters for the deposition of Al/Ti-DLC films.

Target current (A)	Flow rate of Ar (sccm)	LIS current (A)	LIS voltage (V)	Flow rate of C_2H_2 (sccm)	Substrate bias (V)	Deposition pressure (mTorr)
2.5	70	0.2	1100 ± 50	38	−50	4.5

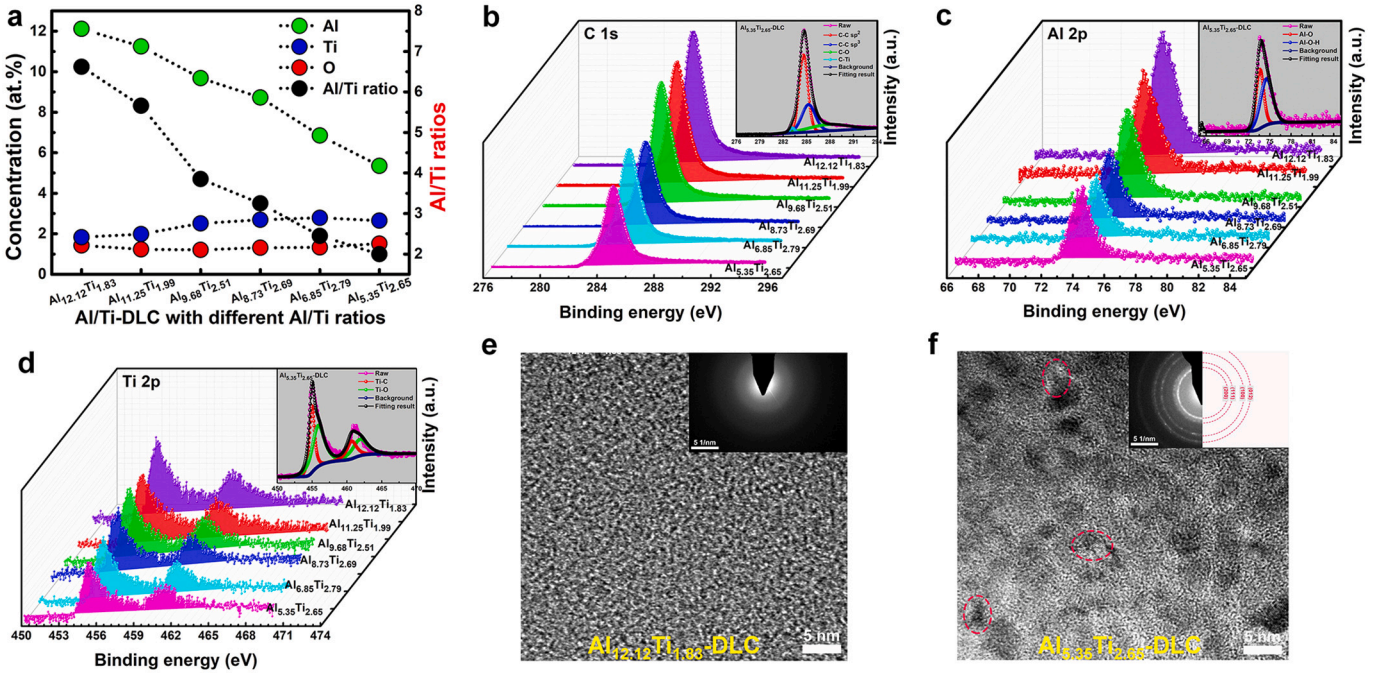

Fig. 2. Chemical composition and microstructure of Al/Ti-DLC films. (a) Composition; (b) C 1s XPS spectra, in which the inset is the deconvoluted result of C 1s spectrum; (c) Al 2p XPS spectra, in which the inset is the deconvoluted result of Al 2p spectrum; (d) Ti 2p XPS spectra, in which the inset is the deconvoluted result of Ti 2p spectrum; (e) and (f) are the HR-TEM images of $Al_{12.12}Ti_{1.83}$-DLC and $Al_{5.35}Ti_{2.65}$-DLC, respectively, and the insets are the corresponding SAED patterns.

under cathodic protection condition was also carried out for each film to quantify the contribution of pure mechanical wear to the total loss of material.

3. Result and discussion

3.1. Composition and microstructure

Fig. 2a displays the chemical composition of Al/Ti-DLC films according to the XPS analysis. It can be seen that the Al content obviously decreases from 12.12 to 5.35 at.%, but there is only a slight increase of Ti content from 1.83 to 2.65 at.%. This indicates that the Al/Ti-DLC films with the Al/Ti ratio changed from 6.6 to 2.0 are achieved. The difference in Al and Ti contents attributes to the higher sputtering yield of Al atoms than Ti atoms [15,21]. In addition, the values of film thickness with Al/Ti ratio are kept at 1.37 ± 0.15 μm, so the influence of film thickness on the structure and tribocorrosion property can be negligible.

The XPS spectra of Al/Ti-DLC films are displayed in Fig. 2b, c, and d, respectively. First, each C 1s spectrum in Fig. 2b shows a major peak at 284.5 eV, indicating the existence of the amorphous carbon [22]. It is further fitted into four peaks, as illustrated in the inset of Fig. 2b, which are located at 283.2 eV for Ti−C bond, 284.6 eV for C−C bond with sp^2 hybridization, 285.3 eV for C−C bond with sp^3 hybridization, and 287.7 eV for C−O bond, respectively [23–25]. Moreover, each Al 2p spectrum (Fig. 2c) is also divided into two peaks (inset of Fig. 2c): one at 74.5 eV representing the Al−O bond and the other at about 73.6 eV corresponding to the Al-O-H bond [21,26]. In addition, Fig. 2d reveals that the Ti 2p XPS spectrum of each film consists of two pairs of peaks, including the one at 455.0 and 460.7 eV is contributed by Ti−C bond and the other at 456.0 and 462.0 eV is from Ti−O bond. Therefore, XPS analysis indicates that in each film the doped Ti exists in the form of titanium carbide and oxide rather than metallic state and the Al bonds with O to form the oxidized Al clusters because of the existence of oxygen [18,27,28]. Fig. 2e and f illustrate the cross-sectional HR-TEM images and corresponding selected area electron diffraction (SAED) patterns of $Al_{12.12}Ti_{1.83}$-DLC and $Al_{5.35}Ti_{2.65}$-DLC films, respectively. It is clearly observed that for the $Al_{5.35}Ti_{2.65}$-DLC film, many black spots are embedded in the amorphous structure, which are the generated TiC crystallites, as confirmed by the sharp diffraction rings [29]. While the HR-TEM image for $Al_{12.12}Ti_{1.83}$-DLC film shows a typical characteristic of amorphous structure, that is the SAED pattern with broad and diffuse hallows. Previous studies [30,31] have shown that the crystallinity of TiC nanocrystalline was weakened by the incorporated Al metal. So tailoring the Al/Ti ratio affects the growth of TiC hard phase and the evolution of carbon hybridized structure in the film, and thus will result in the significant change of mechanical and tribocorrosion properties.

3.2. Mechanical properties and contact stress

Fig. 3a demonstrates the hardness and elastic modulus of films with various Al/Ti ratios. When the Al/Ti ratio declines to 2.0 from 6.6, the hardness of Al/Ti-DLC film increases to 15.70 from 11.85 GPa monotonously, while the elastic modulus also gradually increases to 175.3 from 123.5 GPa. This ascribes to the increased content of titanium carbide nanocrystallites in the film (Fig. 2f) which can compensate for the destruction of amorphous carbon structure effectively and thus improve the film hardness. However, this will also cause the additionally structural distortion, contributing to the increase of residual stress, as reported in previous study [17]. Furthermore, Fig. 3b shows the variation of both the H/E and H^3/E^2 ratios with Al/Ti ratio, which are closely related to the fracture toughness and plastic deformation resistance of the films, respectively [32–34]. When the Al/Ti ratio declines to 2.0 from 6.6, the H/E ratio shows small change, but the H^3/E^2 ratio increases to 0.15 from 0.1, suggesting the improved toughness of Al/Ti-DLC films, which depends on the different possible binding energies corresponding to the distributions of sp^3 and sp^2 carbon sites [34,35]. In particular, the Hertzian contact stress between counter ball and film, which can be used as a standard to judge the fatigue strength of surface contact, is calculated for each case using the following equation [36]:

$$\delta^3 = \frac{9}{16} \times \frac{1}{R_0}\left(\frac{1-\mu_1^2}{E_1} + \frac{1-\mu_2^2}{E_2}\right)^2 P^2 \quad (2)$$

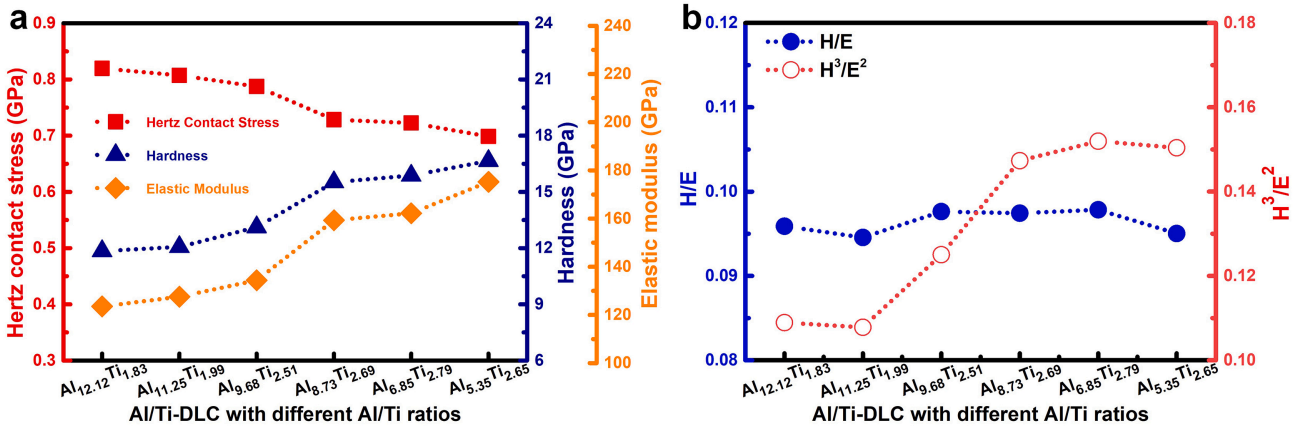

Fig. 3. (a) Mechanical properties and Hertz contact stress, and (b) H/E and H^3/E^2 ratios of films with various Al/Ti ratios.

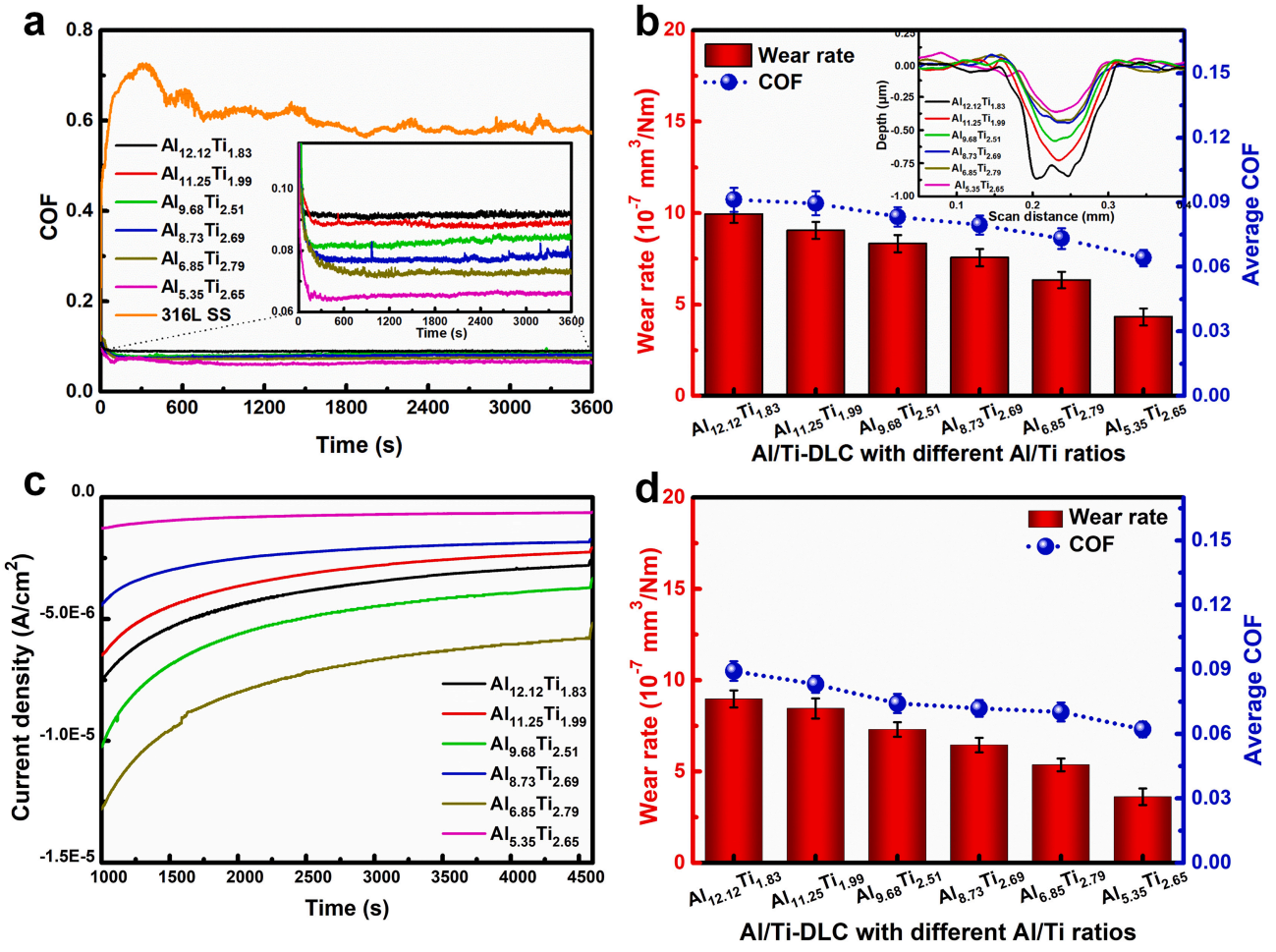

Fig. 4. (a) Friction curves and (b) average wear rate and COF values of films in 3.5 wt% NaCl solution, in which the insets are enlarged friction curves and depth profiles of the wear tracks, respectively. (c) Current evolution curves and (d) average wear rate and COF values of films under cathodic protection conditions.

Table 2
Summary of the loss of Al/Ti-DLC films after tribocorrosion tests.

Sample	V_t (10^{-7} mm^3/Nm)	V_{wc} + V_{cw} (10^{-7} mm^3/Nm)	V_{m0} (10^{-7} mm^3/Nm)	Ratio of (V_{wc} + V_{cw}) to V_t	Ratio of V_{m0} to V_t
$Al_{12.12}Ti_{1.83}$	9.94	0.97	8.97	0.10	0.90
$Al_{11.25}Ti_{1.99}$	9.55	1.10	8.45	0.12	0.88
$Al_{9.68}Ti_{2.51}$	8.33	1.03	7.30	0.12	0.88
$Al_{8.73}Ti_{2.69}$	7.57	1.12	6.45	0.15	0.85
$Al_{6.85}Ti_{2.79}$	6.33	0.97	5.36	0.15	0.85
$Al_{5.35}Ti_{2.65}$	4.33	0.72	3.61	0.17	0.83

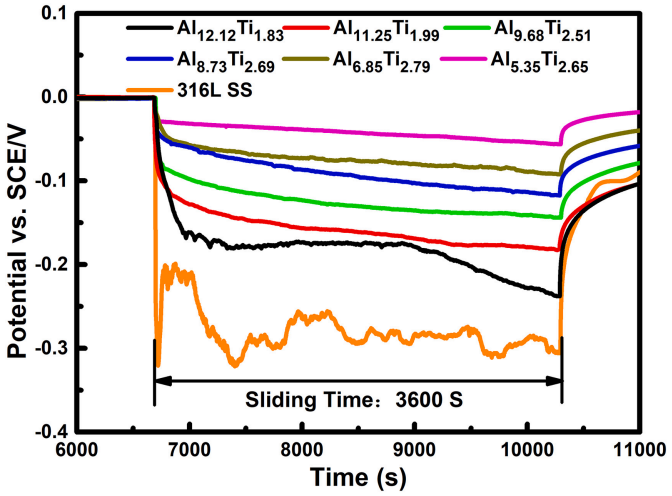

Fig. 5. Evolution of OCP with time for Al/Ti-DLC films in the tribocorrosion test. The result for 316L SS is also considered for comparison.

where E_1, R_0, and μ_1 are the elastic modulus, radius, and Poisson's ratio of Si_3N_4 counter ball, respectively, while E_2 is the elastic modulus of the film; P is the applied normal load. Fig. 3a shows that when reducing the Al/Ti ratio from 6.6 to 2.0, the Hertz contact stress between grinding ball and mated film also decreases from 0.82 to 0.70 GPa. Note that under the same applied load, the Hertzian contact stress experienced by the film is proportional to the Al/Ti ratio, indicating that the higher the Al/Ti ratio, the higher the Hertzian contact stress is. The difference in Hertzian contact stress affects the tribocorrosion performance of films significantly, as will be discussed later.

3.3. Tribocorrosion behavior

The tribocorrosion test of each film is conducted in 3.5 wt% NaCl solution under open circuit potential condition in order to reveal its dependence on the Al/Ti ratio. Fig. 4a shows the typical friction curve for each film, in which the result from bare 316L SS is also considered for comparison. First, compared to the bare case, the deposition of Al/Ti-DLC film onto the metal surface can significantly reduce the COF. Especially, the Al/Ti-DLC can reach the stable friction stage quickly without the running-in process as long as the bare 316L SS. According to the depth profiles of wear tracks (inset of Fig. 4b), the average wear rate and COF values are calculated, as given in Fig. 4b. Following the reduction of Al/Ti ratio, both the average COFs and wear rates of Al/Ti-DLC films drop gradually. When the Al/Ti ratio is 2.0, the minimal COF (0.06) and wear rate (4.33×10^{-7} mm^3/Nm) are achieved, which are discounted by 33% and 56%, respectively, compared to the case with the Al/Ti ratio of 6.6.

It is well known that during the tribocorrosion process, the total volume loss, V_t, of DLC film results from the synergistic effect of mechanical wear and electrochemical corrosion, which can be divided as follows [37,38]:

$$V_t = V_c + V_m = (V_{c0} + V_{cw}) + (V_{w0} + V_{wc}) \quad (3)$$

where V_c represents the loss of material brought by corrosion, which is contributed by pure corrosion (V_{c0}) and wear-induced corrosion (V_{cw}), respectively; V_m represents the loss of material resulted from mechanical wear, including the pure mechanical wear (V_{w0}) and corrosion-induced wear (V_{wc}) separately. Compared to other components in Eq. (3), the contribution of pure corrosion (V_{c0}) to the total loss is very small, which can be negligible. Hence, Eq. (3) can be simplified as follows:

$$V_t = V_{w0} + V_{cw} + V_{wc} \quad (4)$$

In order to expose the percentage of each term in Eq. (4), especially the synergistic effect ($V_{cw} + V_{wc}$), to the total tribocorrosion loss, the tribological test under cathodic protection condition is required to quantify the loss of material induced by mechanical wear only. Before that, the potential value of cathodic protection needs to be defined first. In our previous study [17], the corrosion potential values with Al/Ti ratio varies from −0.07 to 0.20 V versus. SCE. Consequently in the present work, the potential of cathodic protection, −0.5 V versus. OCP, is considered. Fig. 4c displays the corresponding current evolution curves of Al/Ti-DLC films under this potential. It confirms that all the films exhibit relatively small and stable current density values during the whole friction process, suggesting that there is only pure mechanical wear occurred at the friction interface.

Fig. 4d shows the wear rate and COF values of films under cathodic protection conditions. It is found that following the decrease of the Al/Ti ratio from 6.6 to 2.0, the wear rate also presents a significant reduction, which drops from 8.97×10^{-7} to 3.61×10^{-7} mm^3/Nm, and the COF decreases from 0.09 to 0.06. However, by comparing with the results under tribocorrosion condition (Fig. 4b), the COF of each film under cathodic protection condition almost has no change, but there is an obvious reduction of wear rate. This is related to the generation of corrosion product, Al_2O_3, during the friction process, which causes additional abrasive wear, as reported by previous work [17]. Moreover, the specific contribution from the synergistic effect between corrosion and mechanical wear is summarized in Table 2. Note that although the pure mechanical wear dominates the total loss of tribocorrosion volume for each case, the ratio of synergistic effect to total wear loss increases from 10% to 17% when changing the Al/Ti ratio from 6.6 to 2.0. This implies the enhanced corrosion effect and weakened mechanical wear during the tribocorrosion process.

3.4. OCP and EIS analysis

OCP, which is recorded in the tribocorrosion test, is a mixed potential, representing the combined state of worn and unworn materials in the wear track. So it is normally used to assess the corrosion resistance and stability of samples [39,40]. Fig. 5 illustrates the evolution of OCP with time for each film and the result for 316L SS is also provided for comparison. For the uncoated 316L SS, at the initial stage of tribocorrosion test, a sharp decrease in the OCP curve vs time is observed because of the surface activation caused by mechanical effects [14,41]. During the tribocorrosion process, the OCP of 316L SS displays a relatively stable state with serious fluctuation. This is because when the sliding counterpart exerts a force on the metal surface, the mechanical wear destroys the passivated oxide film on the contact surface, but it can also be immediately re-oxidized by the corrosion solution. Therefore, it reflects a dynamic equilibrium of de-passivation and re-passivation at the metal surface [11,42]. After sliding, the OCP of 316L SS gradually increases quickly due to the re-passivation of the metal surface.

However, the Al/Ti-DLC film demonstrates an obvious positive deviation of OCP value without serious fluctuation compared to the 316L SS, indicating better corrosion resistance. In particular, with decreasing the Al/Ti ratio, the OCP value of Al/Ti-DLC film increases gradually, reflecting the enhanced tribocorrosion resistance against both the corrosion attack and mechanical wear. This is consistent with the results of Hertz contact stress and wear rate in the corrosive environment, as given in Figs. 3a and 4b, respectively.

Fig. 6 gives the EIS results including the Nyquist and Bode plots in 3.5 wt% NaCl solution before and after friction sliding. It can be seen that compared to the results before sliding, there is an obvious decrease in the capacitive arc radius of Al/Ti-DLC film after sliding, suggesting that the mechanical damage at the mated friction interface accelerates the electrochemical corrosion, which is also confirmed by the decrease of impedance value in the low-frequency region of Bode diagram. In particular, when the Al/Ti ratio is tailored from 6.6 to 2.0, the magnitude of change in impedance values, which are obtained before and

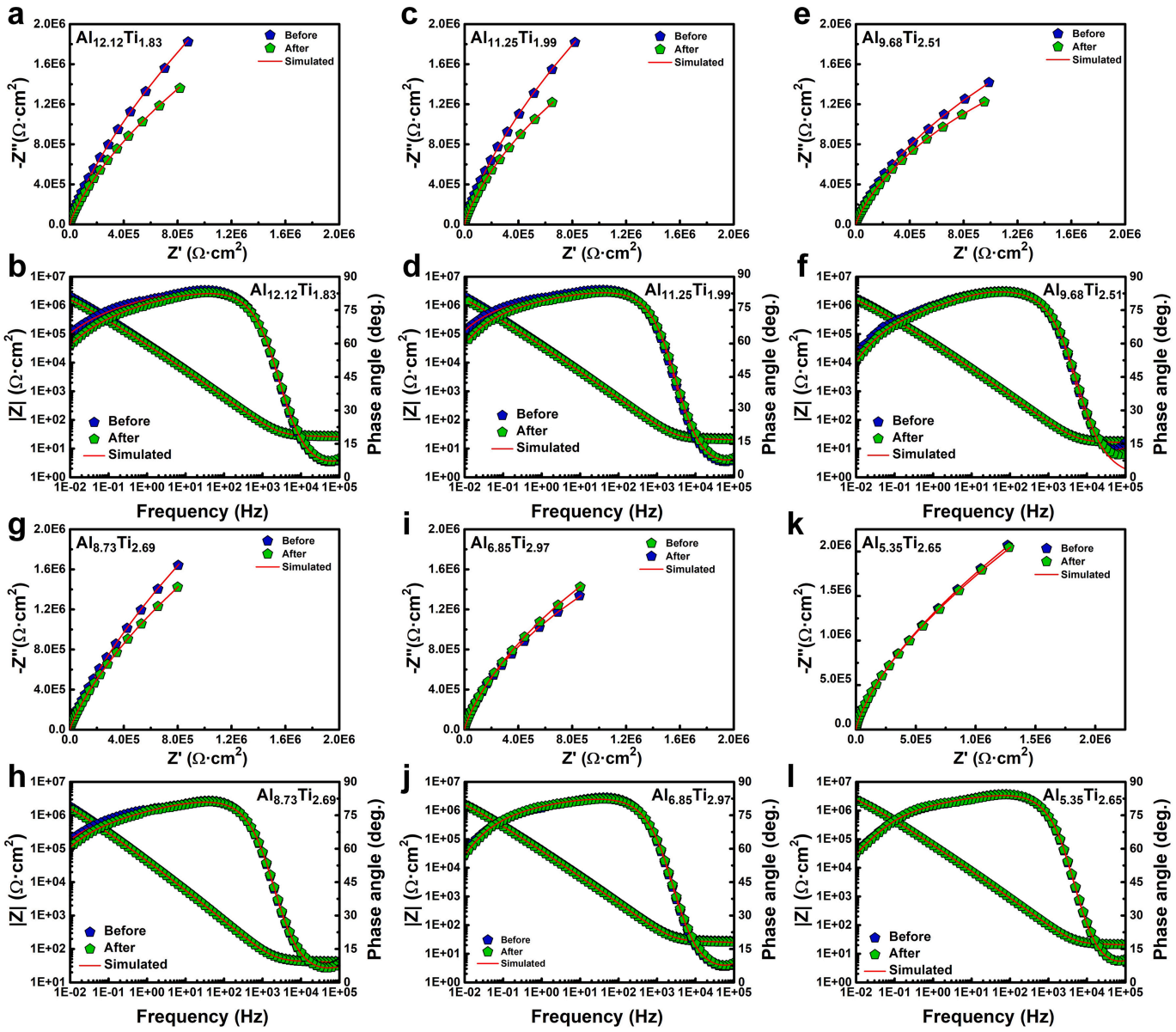

Fig. 6. EIS results of Al/Ti-DLC films before and after sliding processes, respectively, in which (a), (c), (e), (g), (i), and (k) are Nyquist diagrams, while (b), (d), (f), (h), (j), and (l) are Bode diagrams.

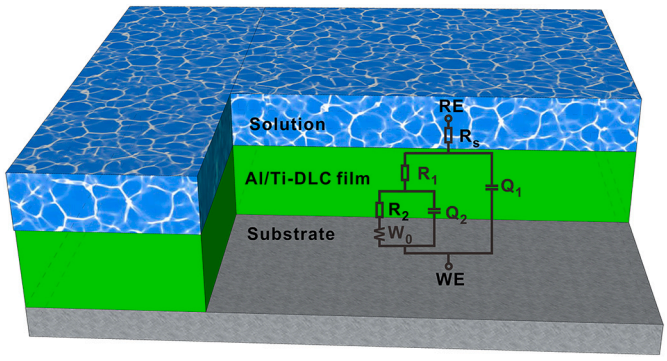

Fig. 7. EC diagram of Al/Ti-DLC film fitted by EIS data.

after sliding processes, respectively, decreases due to the weakened mechanical wear, as illustrated in Fig. 4d and Table 2.

Furthermore, in order to further analyze the electrochemical impedance for each case, the EC fitting is conducted using ZSimpWin software. With respect to the equivalent circuit model of Al/Ti-DLC films, an EC diagram possessing two time constants, labeled as $R_s(Q_1R_1(Q_2R_2W_0))$, is used to reflect the EIS data, as shown in Fig. 7. In this EC model, R_s is the solution resistance; Q_1 and R_1 stand for the film capacitance and pore resistance, respectively, due to the micro defects, impurity, and so on [43,44]; Q_2 and R_2 correspond to the double layer capacitance and transfer resistance of charge separately, which are generated as the solution reaches the interface between film and substrate. In addition, W_0 represents the Warburg impedance, involving the diffusion of the corrosive medium through nano- or micro-pores from the solution to the film/substrate interface.

Fig. 8 presents the fitted value of each component in the EC model (Fig. 7) of Al/Ti-DLC film before and after sliding processes, respectively. First, compared to the fitted results before sliding, after the tribocorrosion test, the n_2 and R_2 values decrease slightly, corresponding to the reduced capacitance characteristics and thus lowering the potential barrier for the diffusion of ion through the film; in addition, the W_0 value also decreases, indicating the high diffusion rate of corrosive ions. These indicate that after the tribocorrosion test, the corrosion

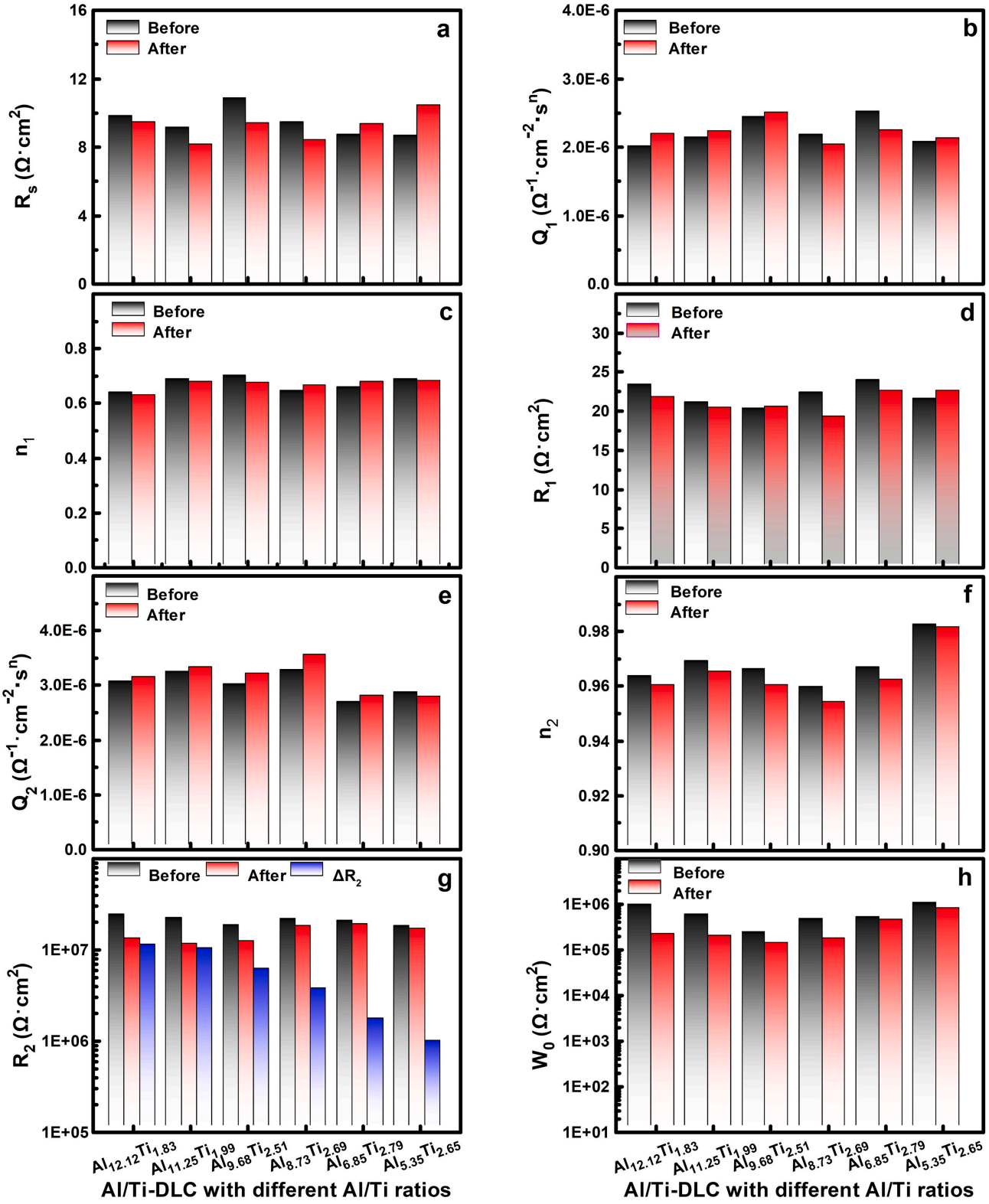

Fig. 8. Fitting results of EIS data before and after tribocorrosion tests, including (a) R_s, (b) Q_1, (c) n_1, (d) R_1, (e) Q_2, (f) n_2, (g) R_2 and (h) W_0.

resistance is weakened for each film due to the presence of mechanical wear. Most importantly, it is also observed that for all Al/Ti-DLC films, the difference in fitted parameters of EC models, obtained before and after sliding processes, exhibits close dependence on Al/Ti ratio. Taking the R_2 value for example, its deviation between before and sliding processes, ΔR_2, is calculated, as given in Fig. 8g. It is found that when the Al/Ti ratio is small, such as 2.0, the ΔR_2 value is 0.86×10^6 $\Omega \cdot cm^2$, while it increases to 0.98×10^7 $\Omega \cdot cm^2$ for that with Al/Ti ratio of 6.6. This illustrates that as Al/Ti ratio increases from 2.0 to 6.6, the aggravated mechanical wear (Fig. 4d) induces the generation and expansion of defects and pores, accelerating the diffusion of corrosive ions into the interface [45,46].

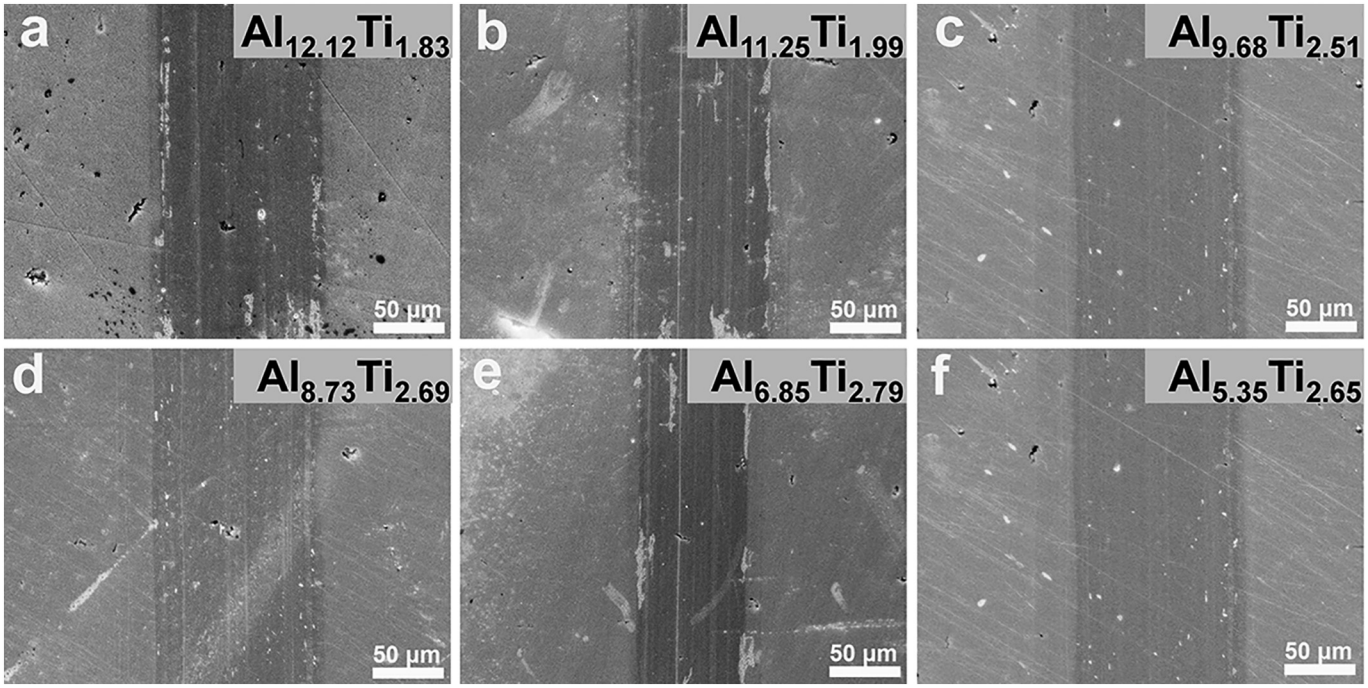

Fig. 9. Wear track morphologies of Al/Ti-DLC films after the tribocorrosion test.

In addition, Fig. 9 further demonstrates the morphologies of wear tracks for Al/Ti-DLC films after tribocorrosion tests. It shows that the wear track of film with a high Al/Ti ratio has more pore defects than that with a low Al/Ti ratio, suggesting the accelerated corrosion induced by wear which agrees well with the EIS analysis (Fig. 8). Combined with the results in Table 2, the increase of synergistic effect between corrosion and wear with Al/Ti ratio (from 6.6 to 2.0) mainly ascribes to the corrosion-induced wear, but the pure mechanical wear is still the main aspect accounting for the drop of tribocorrosion resistance of Al/Ti-DLC films.

4. Conclusion

In this work, the Al/Ti-DLC films with various Al/Ti ratios were successfully fabricated by the HIB system. Combined with the microstructure analysis, the influence of the Al/Ti ratio on mechanical, electrochemical corrosion, and tribocorrosion behaviors was evaluated. Results indicated that following the Al/Ti ratio reduced to 2.0 from 6.6, the mechanical property, including hardness and elastic modulus, was improved because of the increased fractions of titanium carbide and sp^2-C in the film, while the Hertz contact stress between grinding ball and film decreased from 0.82 to 0.70 GPa. Tribocorrosion tests exhibited that both the COF and wear rate of films as a function of Al/Ti ratio from 6.6 to 2.0 reduced obviously. In particular, although the loss of the material was mainly dominated by pure mechanical wear, the contribution from the synergistic effect between corrosion attack and mechanical wear increased following the drop of the Al/Ti ratio. Further electrochemical analysis before and after sliding processes indicated that the mechanical wear accelerated the electrochemical corrosion of Al/Ti-DLC film, but this change was weakened significantly by changing the Al/Ti ratio to 2.0 from 6.6. This suggested that the increase of synergistic effect originated from the corrosion-induced wear. These results shed light on the tribocorrosion behavior of Al/Ti-DLC film and its dependence on the Al/Ti ratio, providing guidance for the selection and design of DLC film for marine applications.

CRediT authorship contribution statement

Xiaowei Xu: Conceptualization, Data curation, Formal analysis, Methodology, Investigation, Visualization, Writing - original draft.**Peng Guo:**Formal analysis, Methodology, Investigation, Writing - original draft.**Xiao Zuo:**Formal analysis, Writing - original draft.**Lili Sun:**Formal analysis, Writing - original draft.**Xiaowei Li:**Conceptualization, Data curation, Funding acquisition, Investigation, Resources, Supervision, Writing - original draft, Writing - review & editing.**Kwang-Ryeol Lee:**Writing - review & editing, Funding acquisition.**Aiying Wang:**Conceptualization, Supervision, Writing - review & editing, Funding acquisition, Resources.

Declaration of competing interest

We declare that we have no financial and personal relationships with other people or organizations that can inappropriately influence our work, there is no professional or other personal interest of any nature or kind in any product, service and/or company that could be construed as influencing the position presented in, or the review of, the manuscript entitled.

Acknowledgments

The authors acknowledged financial support provided by the National Natural Science Foundation of China (51772307), Ningbo Science and Technology Innovation Project (2018B10014), A-class pilot of the Chinese Academy of Sciences (XDA22010303), National Science and Technology Major Project (2017-VII-0013-0110), and K.C. Wong Education Foundation (GJTD-2019-13). Xiaowei Li and Kwang-Reyol Lee would also thank the support from the Korea Research Fellowship Program funded by the Ministry of Science and ICT through the National Research Foundation of Korea (2017H1D3A1A01055070).

References

[1] M.M. Quazi, M.A. Fazal, A.S.M.A. Haseeb, F. Yusof, H.H. Masjuki, A. Arslan, Laser-

based surface modifications of aluminum and its alloys, Crit. Rev. Solid State Mater. Sci. 41 (2015) 106–131.
[2] A. Grill, Diamond-like carbon coatings as biocompatible materials—an overview, Diam. Relat. Mater. 12 (2003) 166–170.
[3] P.F. Macário, A. Vieira, L. Manfroi, M.G.P. da Silva, P. Leite, L. Vieira, Corrosion behavior of Al2024-T3, Al5052-H32, and Al6061-T6 aluminum alloys coated with DLC films in aviation fuel medium, Jet A-1 and AVGAS 100LL, Mater. Corros. 70 (2019) 2278–2291.
[4] R.J.K. Wood, Marine wear and tribocorrosion, Wear 376-377 (2017) 893–910.
[5] M.A. Hafeez, A. Inam, M.A. Arshad, Investigation on microstructural, mechanical, and electrochemical properties of water, brine quenched and tempered low carbon steel, Mater. Res. Express 6 (2019) 096524.
[6] S. Gkatzogiannis, J. Weinert, I. Engelhardt, P. Knoedel, T. Ummenhofer, Correlation of laboratory and real marine corrosion for the investigation of corrosion fatigue behaviour of steel components, Int. J. Fatigue 126 (2019) 90–102.
[7] R.P.C. Costa, D.A. Lima-Oliveira, F.R. Marciano, A.O. Lobo, E.J. Corat, V.J. Trava-Airoldi, Comparative study of the tribological behavior under hybrid lubrication of diamond-like carbon films with different adhesion interfaces, Appl. Surf. Sci. 285 (2013) 645–648.
[8] N. Yamauchi, K. Demizu, N. Ueda, N.K. Cuong, T. Sone, Y. Hirose, Friction and wear of DLC films on magnesium alloy, Surf. Coat. Technol. 193 (2005) 277–282.
[9] S. Neuville, Selective carbon material engineering for improved MEMS and NEMS, Micromachines (Basel) 10 (2019) 539.
[10] F. Pougoum, J. Qian, L. Martinu, J. Klemberg-Sapieha, Z. Zhou, K.Y. Li, S. Savoie, R. Lacasse, E. Potvin, R. Schulz, Study of corrosion and tribocorrosion of Fe3Al-based duplex PVD/HVOF coatings against alumina in NaCl solution, Surf. Coat. Technol. 357 (2019) 774–783.
[11] Y. Ye, Y. Wang, X. Ma, D. Zhang, L. Wang, X. Li, Tribocorrosion behaviors of multilayer PVD DLC coated 304L stainless steel in seawater, Diam. Relat. Mater. 79 (2017) 70–78.
[12] M. Cui, J. Pu, J. Liang, L. Wang, G. Zhang, Q. Xue, Corrosion and tribocorrosion performance of multilayer diamond-like carbon film in NaCl solution, RSC Adv. 5 (2015) 104829–104840.
[13] J. Pu, J. Wang, D. He, S. Wan, Corrosion and tribocorrosion behaviour of super-thick diamond-like carbon films deposited on stainless steel in NaCl solution, Surf. Interface Anal. 48 (2016) 360–367.
[14] J. Liu, X. Wang, B.J. Wu, T.F. Zhang, Y.X. Leng, N. Huang, Tribocorrosion behavior of DLC-coated CoCrMo alloy in simulated biological environment, Vacuum 92 (2013) 39–43.
[15] X. Li, P. Guo, L. Sun, X. Zuo, D. Zhang, P. Ke, A. Wang, Ti/Al co-doping induced residual stress reduction and bond structure evolution of amorphous carbon films: an experimental and ab initio study, Carbon 111 (2017) 467–475.
[16] T. Guo, C. Kong, X. Li, P. Guo, Z. Wang, A. Wang, Microstructure and mechanical properties of Ti/Al co-doped DLC films: dependence on sputtering current, source gas, and substrate bias, Appl. Surf. Sci. 410 (2017) 51–59.
[17] X. Xu, Y. Zhou, L. Liu, P. Guo, X. Li, K.-R. Lee, P. Cui, A. Wang, Corrosion behavior of diamond-like carbon film induced by Al/Ti co-doping, Appl. Surf. Sci. 509 (2020) 144877.
[18] Y. Zhou, P. Guo, L. Sun, L. Liu, X. Xu, W. Li, X. Li, K.-R. Lee, A. Wang, Microstructure and property evolution of diamond-like carbon films co-doped by Al and Ti with different ratios, Surf. Coat. Technol. 361 (2019) 83–90.
[19] X. Yu, X. Zhang, C.-b. Wang, M. Hua, L.-g. Wang, A tribological study of tetrahedral amorphous carbon films prepared by filtered cathodic vacuum arc technique, Vacuum 75 (2004) 231–236.
[20] J. Qi, L. Wang, Y. Wang, J. Pu, F. Yan, Q. Xue, The tribological performance of selected solid lubricant films in sand-dust environments, Wear 271 (2011) 899–910.
[21] X. Pang, L. Shi, P. Wang, Y. Xia, W. Liu, Effects of Al incorporation on the mechanical and tribological properties of Ti-doped a-C:H films deposited by magnetron sputtering, Curr. Appl. Phys. 11 (2011) 771–775.
[22] L. Sun, X. Zuo, P. Guo, X. Li, P. Ke, A. Wang, Role of deposition temperature on the mechanical and tribological properties of Cu and Cr co-doped diamond-like carbon films, Thin Solid Films 678 (2019) 16–25.
[23] W. Dai, P. Ke, M.-W. Moon, K.-R. Lee, A. Wang, Investigation of the microstructure, mechanical properties and tribological behaviors of Ti-containing diamond-like carbon films fabricated by a hybrid ion beam method, Thin Solid Films 520 (2012) 6057–6063.
[24] R.A. Alawajji, G.K. Kannarpady, Z.A. Nima, N. Kelly, F. Watanabe, A.S. Biris, Electrical properties of multilayer (DLC-TiC) films produced by pulsed laser deposition, Appl. Surf. Sci. 437 (2018) 429–440.
[25] W.J. Yang, T. Sekino, K.B. Shim, K. Niihara, K.H. Auh, Deposition and microstructure of Ti-containing diamond-like carbon nanocomposite films, Thin Solid Films 473 (2005) 252–258.
[26] W. Dai, J. Liu, D. Geng, P. Guo, J. Zheng, Q. Wang, Microstructure and property of diamond-like carbon films with Al and Cr co-doping deposited using a hybrid beams system, Appl. Surf. Sci. 388 (2016) 503–509.
[27] C. Kong, P. Guo, L. Sun, Y. Zhou, Y. Liang, X. Li, P. Ke, K.-R. Lee, A. Wang, Tribological mechanism of diamond-like carbon films induced by Ti/Al co-doping, Surf. Coat. Technol. 342 (2018) 167–177.
[28] Y. Guo, P. Guo, L. Sun, X. Li, P. Ke, Q. Li, A. Wang, Tribological properties of Ti-doped diamond-like carbon coatings under dry friction and PAO oil lubrication, Surf. Interface Anal. 51 (2019) 361–370.
[29] F.S. Alencastro, E. Santos, M.E. Mendoza, J.R. Araújo, S. Suarez, B.S. Archanjo, R.A. Simão, Hardening of Al thin films by Ti C doping, Surf. Coat. Technol. 325 (2017) 650–655.
[30] S. Zhou, L. Wang, Q. Xue, Duplex doped nanocomposite carbon-based coating with self-lubricating performance, Diam. Relat. Mater. 21 (2012) 58–65.
[31] S. Zhou, L. Wang, S.C. Wang, Q. Xue, Comparative study of simplex doped nc-WC/a-C and duplex doped nc-WC/a-C(Al) nanocomposite coatings, Appl. Surf. Sci. 257 (2011) 6971–6979.
[32] N.A. Sakharova, J.V. Fernandes, M.C. Oliveira, J.M. Antunes, Influence of ductile interlayers on mechanical behaviour of hard coatings under depth-sensing indentation: a numerical study on TiAlN, J. Mater. Sci. 45 (2010) 3812–3823.
[33] A. Amanov, T. Watabe, R. Tsuboi, S. Sasaki, Improvement in the tribological characteristics of Si-DLC coating by laser surface texturing under oil-lubricated point contacts at various temperatures, Surf. Coat. Technol. 232 (2013) 549–560.
[34] S. Neuville, A. Matthews, A perspective on the optimisation of hard carbon and related coatings for engineering applications, Thin Solid Films 515 (2007) 6619–6653.
[35] M.A. Tamor, W.C. Vassell, K.R. Carduner, Atomic constraint in hydrogenated diamond-like carbon, Appl. Phys. Lett. 58 (1991) 592–594.
[36] H.-X. Song, L.-L. Ke, J. Su, J. Yang, S. Kitipornchai, Y.-S. Wang, Surface effect on the contact problem of a piezoelectric half-plane, Int. J. Solids Struct. 185-186 (2020) 380–393.
[37] J.P. Celis, P. Ponthiaux, F. Wenger, Tribo-corrosion of materials: interplay between chemical, electrochemical, and mechanical reactivity of surfaces, Wear 261 (2006) 939–946.
[38] A. Mäntyranta, V. Heino, E. Isotahdon, T. Salminen, E. Huttunen-Saarivirta, Tribocorrosion behaviour of two low-alloy steel grades in simulated waste solution, Tribol. Int. 138 (2019) 250–262.
[39] M. Li, Y.B. Wang, X. Zhang, Q.H. Li, Q. Liu, Y. Cheng, Y.F. Zheng, T.F. Xi, S.C. Wei, Surface characteristics and electrochemical corrosion behavior of NiTi alloy coated with IrO2, Mater. Sci. Eng. C Mater. Biol. Appl. 33 (2013) 15–20.
[40] J. Wei, H. Li, L. Liu, P. Guo, P. Ke, A. Wang, Enhanced tribological and corrosion properties of multilayer ta-C films via alternating sp3 content, Surf. Coat. Technol. 374 (2019) 317–326.
[41] R. Bayón, A. Igartua, J.J. González, U. Ruiz de Gopegui, Influence of the carbon content on the corrosion and tribocorrosion performance of Ti-DLC coatings for biomedical alloys, Tribol. Int. 88 (2015) 115–125.
[42] Y. Yan, A. Neville, D. Dowson, S. Williams, J. Fisher, Effect of metallic nanoparticles on the biotribocorrosion behaviour of Metal-on-Metal hip prostheses, Wear 267 (2009) 683–688.
[43] X.-J. Cui, C.-M. Ning, L.-L. Shang, G.-A. Zhang, X.-Q. Liu, Structure and anticorrosion, friction, and wear characteristics of pure diamond-like carbon (DLC), Cr-DLC, and Cr-H-DLC films on AZ91D Mg alloy, J. Mater. Eng. Perform. 28 (2019) 1213–1225.
[44] H.-G. Kim, S.-H. Ahn, J.-G. Kim, S.J. Park, K.-R. Lee, Effect of Si-incorporation on wear–corrosion properties of diamond-like carbon films, Thin Solid Films 482 (2005) 299–304.
[45] D.D. Xiang, X.D. Sui, X.P. Tan, J.Y. Hao, Z.W. Wang, Z.H. Liao, W.Q. Liu, S.B. Tor, Improving biotribological properties and corrosion resistance of CoCrMo alloy via a Cr-GLC nanocomposite film in simulated body fluids, Surf. Coat. Technol. 378 (2019) 124840.
[46] T.M. Manhabosco, A.P.M. Barboza, R.J.C. Batista, B.R.A. Neves, I.L. Müller, Corrosion, wear and wear–corrosion behavior of graphite-like a-C:H films deposited on bare and nitrided titanium alloy, Diam. Relat. Mater. 31 (2013) 58–64.